AIP Applied Physics Letters

Semiconductor optical parametric generators in isotropic semiconductor diode lasers

Bhavin J. Bijlani, Payam Abolghasem, and Amr S. Helmy

Citation: Appl. Phys. Lett. **103**, 091103 (2013); doi: 10.1063/1.4819736
View online: http://dx.doi.org/10.1063/1.4819736
View Table of Contents: http://apl.aip.org/resource/1/APPLAB/v103/i9
Published by the AIP Publishing LLC.

Additional information on Appl. Phys. Lett.

Journal Homepage: http://apl.aip.org/
Journal Information: http://apl.aip.org/about/about_the_journal
Top downloads: http://apl.aip.org/features/most_downloaded
Information for Authors: http://apl.aip.org/authors

ADVERTISEMENT

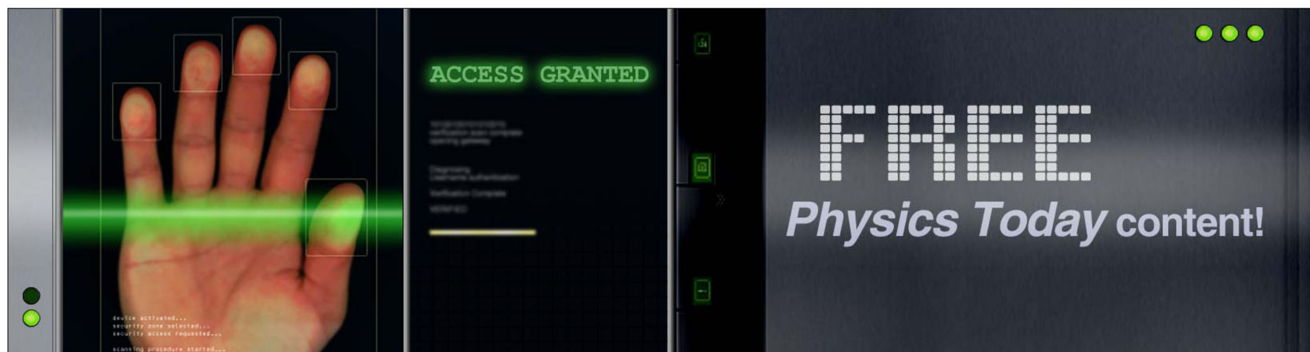

Downloaded 27 Aug 2013 to 142.150.242.148. This article is copyrighted as indicated in the abstract. Reuse of AIP content is subject to the terms at: http://apl.aip.org/about/rights_and_permissions

APPLIED PHYSICS LETTERS **103**, 091103 (2013)

Semiconductor optical parametric generators in isotropic semiconductor diode lasers

Bhavin J. Bijlani, Payam Abolghasem, and Amr S. Helmy[a)]
The Edward S. Rogers Sr. Department of Electrical and Computer Engineering, University of Toronto, 10 King's College Road, Toronto, Ontario M5S 3G4, Canada

(Received 11 July 2013; accepted 15 August 2013; published online 27 August 2013)

We report on the characteristics of an intracavity semiconductor optical parametric generator in multiple-quantum well AlGaAs/InGaAs Bragg reflection waveguide lasers emitting between 986 and 995 nm. The cavity of the laser is phase-matched for down-conversion of pump photons to a signal between 1739 and 1767 nm and an idler between 2235 and 2328 nm. The normalized conversion efficiency is calculated to be 1.23×10^3 %$W^{-1}cm^{-2}$ above laser threshold and 1.25 $\times 10^4$ %$W^{-1}cm^{-2}$ below threshold. The demonstrated device is potential for the realization of integrated parametric devices such as electrically pumped entangled photon-pair sources and optical parametric oscillation, where quantum optical effects can unfold. © *2013 AIP Publishing LLC*. [http://dx.doi.org/10.1063/1.4819736]

Optical nonlinearities in semiconductors play a pivotal role in photonics by providing key functions for a broad spectrum of devices. Second order nonlinear interactions, which are larger in magnitude when compared to their third order counterparts have also been utilized in monolithic semiconductor structures, but on a more limited scale.[1–3] Nonetheless, they have fueled advances in vital fields such as quantum optics, where parametric processes generate and manipulate the quantum state of photons,[4–7] and coherent light sources, where it is used to generate essential wavelengths through frequency-mixing.[2,8] Since their discovery, second order nonlinearities have been chiefly exploited in bulk crystals such as $LiNbO_3$, KTP, and BBO, where useful devices use hybrid materials and utilize free space optical assemblies.[9]

Harnessing the large $\chi^{(2)}$ coefficients of compound semiconductors near the material bandgap efficiently in a monolithic form-factor is attractive for numerous domains of science and technology.[10] Despite their potential, the realization of practical monolithic parametric devices based on $\chi^{(2)}$ nonlinearities in semiconductors has been lagging and was only demonstrated in the mid-infrared using watts of pump power to access resonant intra-band $\chi^{(2)}$ components.[1,2] In these demonstrations, where only difference-frequency generation was achieved, no phase-matching (PM) was utilized since the operating wavelengths are much further from the materials bandgap. Challenges in harnessing bulk $\chi^{(2)}$ near the material bandgap are encountered because semiconductors such as GaAs and InP are optically isotropic with no intrinsic birefringence. Phase-matching the $\chi^{(2)}$ interactions in semiconductors near the bandgap, where $\chi^{(2)}$ is the largest and where also significant dispersion takes place, remains a challenge. Several techniques have been proposed and demonstrated to achieve PM in AlGaAs,[3,11–13] however, none have demonstrated monolithic integration with active components or realization in a diode laser cavity.[10] Harnessing parametric processes on the chip-scale can transform the current capabilities of conducting quantum optical and quantum simulation experiments by mapping them from optical benches into circuits that benefit from the precision obtained through nano-fabrication.

Bragg reflection waveguides (BRWs), which guide modes based on one-dimensional (1D) photonic bandgap structures, have been investigated recently as a new route to attain exact PM in semiconductor waveguides.[10] Seeded parametric processes in BRWs including second-harmonic generation (SHG), sum-frequency generation (SFG), and difference-frequency generation (DFG) have been demonstrated.[14] However, unseeded processes such as parametric fluorescence have not been demonstrated before using electrical excitation. Recently, photon pairs with a high flux, generated through spontaneous parametric down-conversion (SPDC), have been demonstrated via optical excitation using an external pump in BRWs.[15] In addition, edge emitting BRW lasers operating at room temperature with emission around 980 nm have been demonstrated.[16,17]

In this letter, we demonstrate the unique behavior observed in the first all semiconductor optical parametric generators (OPOs). The distinct behavior and in particular the conversion efficiency below threshold and the dispersion of the tuning curve of this semiconductor optical parametric generator are examined and contrasted with the behavior of conventional optical parametric generators. The parametric process was pumped using BRW diode lasers, where bulk $\chi^{(2)}$ nonlinearity is phase-matched for non-degenerate intra-cavity parametric down-conversion using on-chip diode laser pump. The demonstration of this unseeded process, which has significantly lower efficiency compared to its seeded counterparts, using electrical excitation of a few milli-watts in a laser diode cavity, was previously unattainable and enables the realization of this semiconductor optical parametric generator.

A schematic of a BRW laser is illustrated in Fig. 1. The wafer was grown using metal organic chemical vapor deposition (MOCVD) on 2° n-GaAs substrate. The active region of the laser consists of two $In_{0.20}Ga_{0.80}As$ quantum-wells with a well thickness of 6 nm, separated by 10 nm GaAs

a)Electronic mail: a.helmy@utoronto.ca

 © 2013 AIP Publishing LLC

Downloaded 27 Aug 2013 to 142.150.242.148. This article is copyrighted as indicated in the abstract. Reuse of AIP content is subject to the terms at: http://apl.aip.org/about/rights_and_permissions

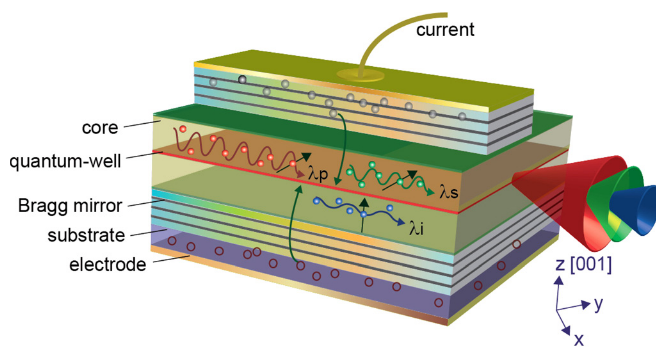

FIG. 1. A schematic of a Bragg reflection waveguide laser. The laser emission serves as the pump for the intra-cavity parametric fluorescence.

barriers. The bottom Bragg reflector is n-doped and consists of five periods of $Al_{0.30}Ga_{0.70}As$/GaAs bi-layers. The top reflector is p-doped and consists of four periods of similar bi-layers to those of the bottom reflector. The core of the structure consists of one layer of $Al_{0.35}Ga_{0.65}As$ with a thickness of 1085 nm.[14] Ridge lasers with a width of 3.5 μm and an etch depth of $\approx$3.6 μm were patterned using plasma etching. The sample under test had a length of 0.98 mm. The laser was biased in pulsed mode with 40 μs pulses width and 20 μs delay. The turn-on voltage of the laser was measured to be 3.5 V with a threshold current of 53 mA and a threshold current density of 1545 A/cm^2.

To characterize the parametric fluorescence, the emission of the laser was collected using a 60$\times$ objective lens. A thermo-electrically cooled InGaAs detector that is phase-locked with an optical chopper at 200 Hz and operated at –30 °C was used to measure the parametric fluorescence (PF) power. Two silicon filters and a long-wavelength pass filter with cut-off around 1650 nm were used to remove the pump before the InGaAs detector. The PF spectrum was examined using a Fourier transform infrared (FTIR) spectrometer.

Initially, the device's spectral behavior was investigated. Figure 2(a) shows typical emission spectra of the diode laser pump measured at various currents. It can be seen from the figure how the pump spectrum affects the spectrum of the parametric light. For a current of 50 mA, which is below the laser threshold ($I_{\rm th} = 53$ mA), the wide spectrum of the pump results in wide band fluorescence. Only the signal spectrum could be observed in this case. The idler spectrum could only be resolved for currents above the pump laser threshold. The examination of the pump spectrum for different injected currents revealed that for currents between 60 and 90 mA the pump emission was mainly in a single transverse mode, whereas at higher injected currents multi-transverse-mode lasing could be observed. The single and multi-mode regimes could be distinguished in the spectra of the signal and idler as shown in Fig. 2(b) for injected currents of 60 mA and 110 mA. In contrast to the case in the single mode regime, the determination of the wavelengths of λ_p, λ_s, and λ_i in the multimode regime is associated with large error bars due to the multimode behavior.

The wavelength tuning curves of the device are shown in Fig. 2(c) where the dependence of λ_s and λ_i on λ_p are plotted. The tuning of λ_p was achieved by changing the injected current. In all published tuning curves to date,[18] λ_s is red shifted with the increase of λ_p while λ_i is blue shifted with the increase of λ_p. The slopes of these tuning curves are chiefly determined by the dispersion of the device. The tuning curves of the monolithic parametric device discussed here exhibit the opposite behavior as can be seen in Fig. 2(c), where λ_s clearly blue shifts with the increase of λ_p, while λ_i clearly red shifts with the increase of λ_p. This behavior is observed for the first time and merits further analysis. The root-causes for this behavior will be elucidated for the tuning curve in the first regime of operation, where the pump laser lases in a single transverse mode. In all previous reports of parametric fluorescence, the nonlinear medium was optically pumped with the laser pump operated in the transparency regime of the medium. As such, any secondary effects of the pump on the medium would mainly include heating and $\chi^{(3)}$ effects. To take into account the semiconductor laser cavity effects on the tuning curve, the dependence of material indices on the device temperature and the free carrier concentration within the intrinsic region of the diode[19,20] should be taken into account as discussed below.

The dependence of refractive index of AlGaAs layers on aluminum concentration, wavelength, and temperature was obtained using the model reported in Ref. 21. The refractive index of the $In_{0.20}Ga_{0.80}As$ well in the active region was obtained from an empirical model. To include the effect of free carrier concentration, the laser was modeled as a $p - i - n$ structure, where the intrinsic region was composed of the undoped region. The carrier lifetime in the intrinsic region was considered to be $\tau = 1.4$ ns.[22,23] The model proposed in Ref. 19 was then used to include the effects of the free carrier concentration on refractive index change including bandgap shrinkage, band filling effect, and free carrier absorption. In order to account for the effects of self-heating and free carrier concentration on wavelength of the PF, it is assumed that the dependence of pump wavelength and device temperature can both be expressed as linear functions of the injected current. For the dependence of the λ_p on current, the measured spectra of the pump at various currents, above laser threshold, were used to extract the linear relation $\lambda_p(I) = 30.56I + 985$ nm. For self-heating effect, the relation between the device temperature and current was expressed as $T = m_T I + h$. The temperature coefficient, m_T, was considered as a fitting parameter in simulations and the value of $h = 20$ °C was determined by the fact that the temperature set point at zero injection was 20 °C in the setup. Figure 2(d) shows the simulated tuning curve when the effects of the simultaneous change in temperature and carrier concentration as functions of injected current are included for three cases where $m_T = 0, 112$, and 445 °C/mA. The values obtained for the fitting parameter m_T translate to a range of junction temperatures between 20 °C and 130 °C. The associated change in λ_p for m_T larger than 400 °C explains the reversal of the slopes of the signal and idler in the tuning curve. While it is customary for carriers to be pinned above threshold for perfect lasers, hetero-barrier leakage can take place leading to a variable carrier concentration above threshold in some devices, as can be seen in this case. Through dispersion control in the cavity along with the effects of changing carrier concentration, it is possible to tune and control this behavior, which offers new opportunities for various applications where such tunability would be required. It should be noted

Downloaded 27 Aug 2013 to 142.150.242.148. This article is copyrighted as indicated in the abstract. Reuse of AIP content is subject to the terms at: http://apl.aip.org/about/rights_and_permissions

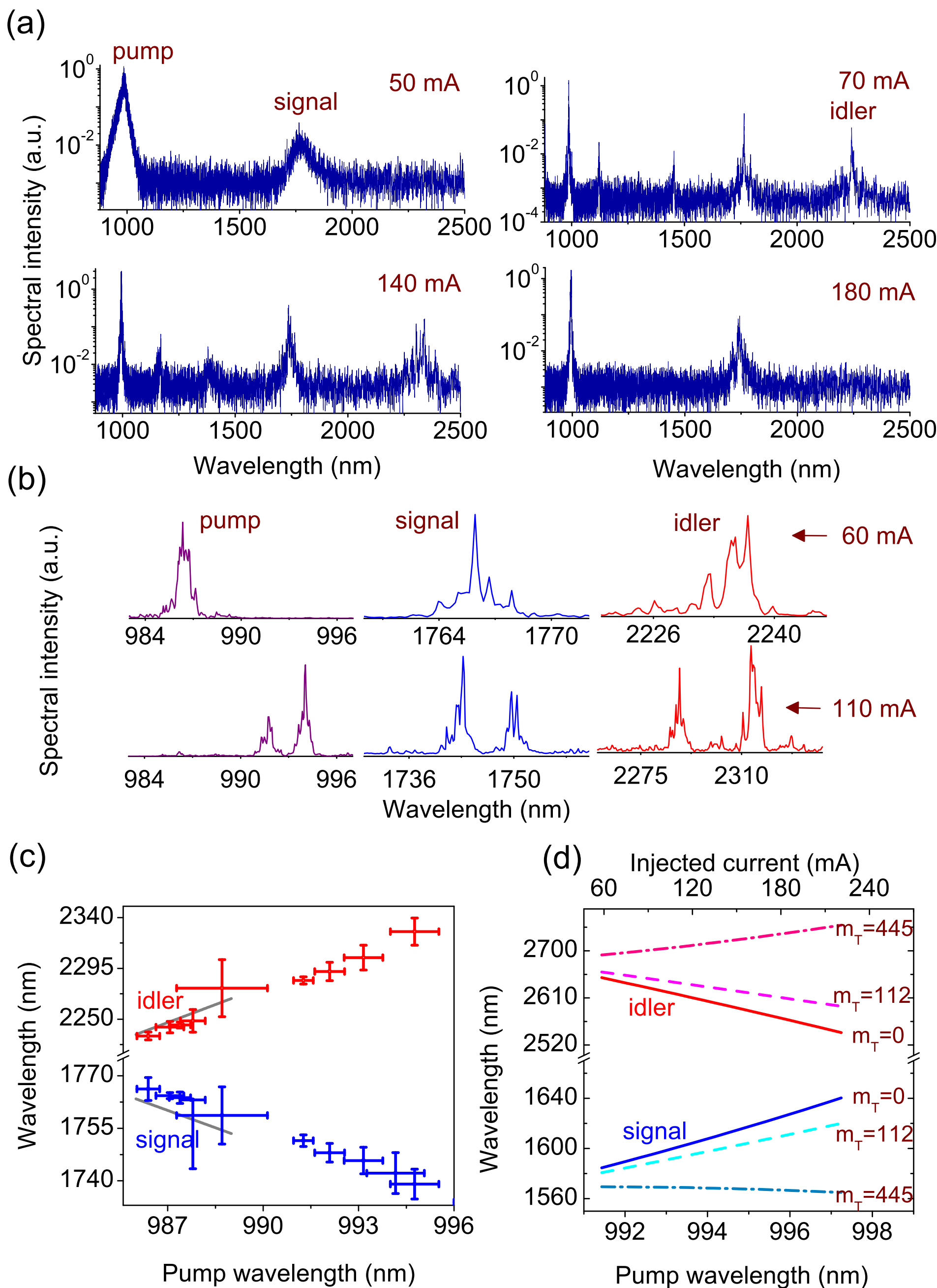

FIG. 2. (a) Spectral intensity of the diode pump for various injection currents. (b) Enlarged spectra of the pump, signal, and idler at currents of 60 mA and 110 mA. For injected currents more than ≈90 mA, the multi-mode lasing is evident. (c) Measured dependence of λ_s and λ_i on λ_p. The solid lines are the simulated curves where device temperature and free carrier concentration are included. (d) Simulated dependences of λ_s and λ_i on λ_p for various temperature coefficients, m_T.

that, while increased device temperature and free carrier effects explain the reverse slope of the PF tuning curves, comparing Figs. 2(c) and 2(d) indicates a mismatch between the experimental and theoretical values of λ_p, λ_s, and λ_i. Such wavelength shift can partly be explained by the shift of the lasing pump wavelength from design value and the effect of the 2D confinement in ridge structures. A detailed study to identify the root-cause of such wavelength shift requires specific device designs where the lasing wavelength can be tuned.

The internal fluorescence power estimated before the exit facet of the diode was extracted by compensating for the transmission of the objective lens used for collecting light, the Fresnel's reflection, the transmission of the filters used to reject the pump before the InGaAs detector, the scaling factor associated with chopping the emission of the laser, and the calibration number associated with converting the pulsed current to an equivalent DC current. The objective lens used had a cut-off wavelength around 2710 nm with a transmission of 0.84 at λ_p. The transmission of the lens, measured using a FTIR spectrometer, at λ_s and λ_i nm were found to be 0.57 and 0.30, respectively. The Fresnel's reflection at pump, signal, and idler wavelengths was considered to be 0.3. The transmission of the long-wavelength pass filter with a cut-off around 1650 nm was measured to be 0.1 and 0.92 at signal and idler wavelengths. The transmission of a single silicon filter was 0.61 at both signal and idler wavelengths. The calibration scaling due to chopping the diode emission at a frequency of 200 Hz was calculated to be 5.55. To estimate the CW equivalent of the measured fluorescence power, P_p was divided by the duty cycle of the pulsed current which was 0.67. The collection efficiency of the objective lens was assumed to be 100%. The dependence of PF power, P_{PF}, on the pump laser power, P_p, is shown in Fig. 3(a). For an injected current of 180 mA, P_{PF} inside the cavity was estimated to be ≈15.3 nW with a pump power of 25 mW. As can

Downloaded 27 Aug 2013 to 142.150.242.148. This article is copyrighted as indicated in the abstract. Reuse of AIP content is subject to the terms at: http://apl.aip.org/about/rights_and_permissions

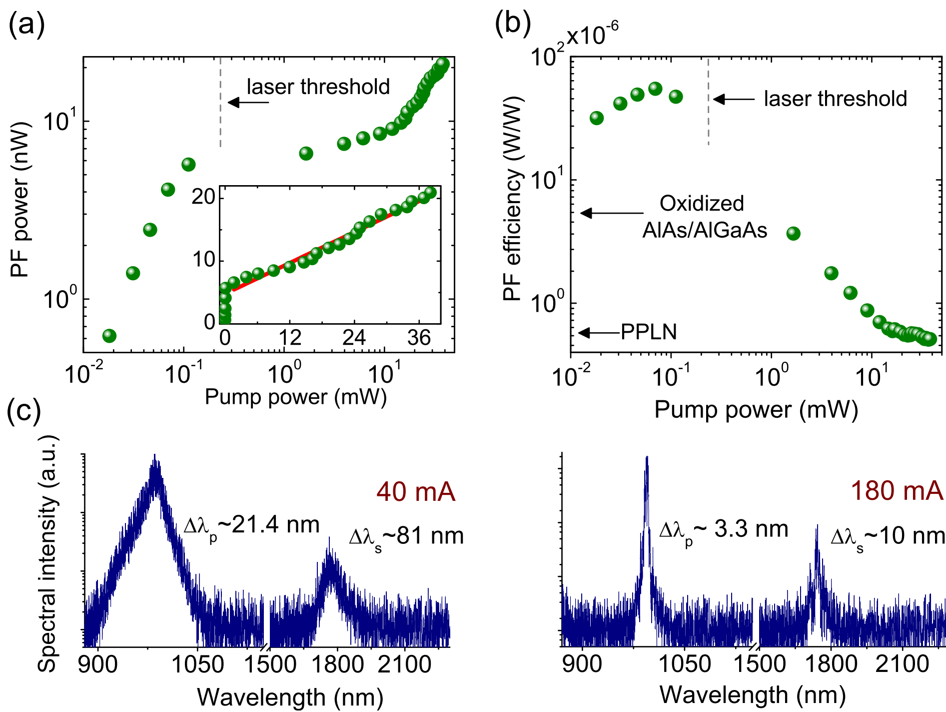

FIG. 3. (a) PF power as a function of pump power plotted in log-log scale. The inset is the same figure plotted in linear scale. The solid-line is a linear fit showing the linear dependence of P_{PF} on P_p for above threshold operation. (b) Dependence of η_{PF} on P_p. The arrows pointing to the vertical axis show the reported efficiencies for oxidized AlAs/AlGaA (see Ref. 24) and PPLN (see Ref. 25) waveguides for comparison. (c) Enlarged spectra of the laser emission at injected currents of 40 mA and 180 mA.

be seen in the plot, there are two slopes associated with operating below and above threshold. The slope of P_{PF} vs. P_p below threshold is significantly larger than that of the above threshold operation. We first focus on the efficiency above threshold and compare it with other nonlinear materials and devices.

The efficiency of parametric fluorescence is defined as, $\eta_{\text{PF}} = P_s/P_p$, where P_s is the fluorescence power in the signal mode. For an injected current of 180 mA, η_{PF} was found to be $\approx 5.7 \times 10^{-7}$ W/W for $P_s = 14.2$ nW. The probability associated with the down-conversion of the high energy pump photons can be estimated as $\eta_{\text{PF}} \times \lambda_s/\lambda_p = 1.0 \times 10^{-6}$ for $\lambda_p = 994$ nm and $\lambda_s = 1743$ nm. Another figure of merit indicating the performance of the device is the normalized conversion efficiency defined as $\eta_{\text{norm}} = P_s/P_p P_i(0)$. $P_i(0)$ is the idler noise power contributing to the generation of the signal power and is defined as $P_i(0) = (\hbar\omega_i/2\pi)\Delta\omega_i$, where $\Delta\omega_i$ is the spectral bandwidth of the idler.[18] For the injected current of 180 mA, the idler bandwidth was estimated to be $\Delta\lambda_i \approx \Delta\lambda_s = 10$ nm ($\Delta\omega_i = 5.2$ THz) at $\lambda_i = 2313$ nm. This results in an idler noise power of $P_i(0) = 48.1$ nW. The normalized conversion efficiency of the device is then calculated to be $\eta_{\text{norm}} = 1.18 \times 10^3$ %W^{-1} or $\eta_{\text{norm}}/L^2 = 1.23 \times 10^3$ %W^{-1}cm^{-2} for devices with a cavity length of $L = 0.98$ cm.

The highest conversion efficiency for parametric fluorescence in AlGaAs devices has been previously reported as $\eta_{\text{norm}}/L^2 = 1.5 \times 10^3$ %W^{-1}cm^{-2} for a passive, externally pumped, form-birefringence waveguide with a cavity length of 3 mm at degeneracy[24] A comparison with PF in other material systems is also noteworthy. For example, in Ref. 25, degenerate PF was observed in a 2 cm long periodically poled $LiNbO_3$ waveguide, where conversion efficiency was determined to be 130 % W^{-1} cm^{-2}; an order of magnitude lower than the efficiency of our device. Also in Ref. 26, non-degenerate PF is reported in a 1.97 mm long quasi-phase-matched GaP waveguide where the conversion efficiency was obtained to be 16 % W^{-1} cm^{-2}.

The dependence of η_{PF} on pump power is shown in Fig. 3(b). From the figure, the PF efficiency increases with pump power when the diode is biased below threshold until it reaches a maximum below threshold. It systematically decreases when operating above laser threshold. The reduction of the efficiency above threshold can be attributed to increased propagation losses with increased current. From the figure, the highest PF efficiency is $\eta_{\text{PF}} \approx 5.44 \times 10^{-5}$ W/W associated with an injected current of 40 mA. The pump and signal power were estimated to be 69.8 μW and 3.8 nW, respectively. At this current, as can be seen in Fig. 3(c), the bandwidth of the signal is measured to be $\Delta\lambda_s = 81$ nm. The idler spectrum could not be resolved at such low current level, and as a rough estimation, we assume that $\Delta\lambda_i \approx \Delta\lambda_s$. The idler noise power is then estimated to be ≈ 434 nW at $\lambda_i = 2231$ nm. This translates to a normalized conversion efficiency of 1.25×10^4 %W^{-1}cm^{-2}.

The steep increase of PF efficiency below the laser threshold is better witnessed in Fig. 3(b), where the dependence of P_{PF} on pump power is plotted in log-log scale. This giant efficiency can be attributed to the pump bandwidth. The pump spectrum below threshold operation is governed by spontaneous emission and is on the order of the gain bandwidth, which is on the order of tens of nanometers. A pump with such a large spectral bandwidth results in a wideband parametric fluorescence, particularly as the PM bandwidth in the down-conversion process for these waveguides is inherently wide. This can be seen when we compare the spectral bandwidth of the pump and down-converted signal below and above the laser threshold. From Fig. 3(c) for 40 mA current injection, the bandwidth of the pump and signal are measured to be $\Delta\lambda_p = 21$ nm and $\Delta\lambda_s = 81$ nm. These parameters were estimated to be 3.3 nm and 10 nm, respectively, at a current of 180 mA. This comparison suggests that while the pump power level below threshold is weak, the fluorescence power can be significant as the PF power is integrated over a larger spectral range. This

Downloaded 27 Aug 2013 to 142.150.242.148. This article is copyrighted as indicated in the abstract. Reuse of AIP content is subject to the terms at: http://apl.aip.org/about/rights_and_permissions

behavior has not been studied previously in other as OPOs pumping nonlinear devices has been chiefly carried out using coherent laser radiation. However, the significant efficiencies observed here suggest that it is a topic that merits further investigation.

In summary, we report the unique properties of the first current injection-based semiconductor optical parametric generator based on a Bragg reflection waveguide laser, where $\chi^{(2)}$ nonlinearity has been phase-matched in a diode laser cavity. The normalized conversion efficiency of the parametric fluorescence is calculated to be 1.23×10^3 %$W^{-1}cm^{-2}$ above threshold and 1.25×10^4 %$W^{-1}cm^{-2}$ below threshold. The values below threshold are remarkably high (at least an order of magnitude higher than the reported record to date). The tuning curve of this class of devices shows dispersion that is opposite in sign in comparison to non-integrated parametric generators. This previously undocumented behavior could be attributed to the interplay of the thermal and carrier injection effects in the cavity.

The authors acknowledge the support of Natural Sciences and Engineering Research Council of Canada (NSERC) for funding this research and CMC Microsystems for growing the wafer. We are grateful to K. Burch and A. Reijnders for making the FTIR spectrometer available for characterization.

[1]E. Rosencher, A. Fiore, B. Vinter, V. Berger, P. Bois, and J. Nagle, Science **271**, 168 (1996).
[2]M. A. Belkin, F. Capasso, A. Belyanin, D. L. Sivco, A. Y. Cho, D. C. Oakley, C. J. Vineis, and G. W. Turner, Nat. Photonics **1**, 288 (2007).
[3]A. Fiore, V. Berger, E. Rosencher, P. Bravetti, and J. Nagle, Nature **391**, 463 (1998).
[4]J. P. Torres, K. Banaszek, and I. A. Walmsley, Prog. Opt. **56**, 227 (2011).
[5]S. L. Braunstein and P. van Loock, Rev. Mod. Phys. **77**, 513 (2005).
[6]R. Ursin, F. Tiefenbacher, T. Schmitt-Manderbach, H. Weier, T. Scheidl, M. Lindenthal, B. Blauensteiner, T. Jennewein, J. Perdigues, P. Trojek, B. Oemer, M. Fuerst, M. Meyenburg, J. Rarity, Z. Sodnik, C. Barbieri, H. Weinfurter, and A. Zeilinger, Nat. Phys. **3**, 481 (2007).
[7]P. G. Kwiat, K. Mattle, H. Weinfurter, A. Zeilinger, A. V. Sergienko, and Y. H. Shih, Phys. Rev. Lett. **75**, 4337 (1995).
[8]Q. Y. Lu, N. Bandyopadhyay, S. Slivken, Y. Bai, and M. Razeghi, Appl. Phys. Lett. **99**, 131106 (2011).
[9]M. P. De Micheli, Quantum Semiclassic. Opt. **9**, 155 (1997).
[10]A. S. Helmy, P. Abolghasem, J. S. Aitchison, B. J. Bijlani, J. Han, B. H. Holmes, D. C. Hutchings, U. Younis, and S. J. Wagner, Laser Photonics Rev. **5**, 272 (2011).
[11]K. Moutzouris, S. V. Rao, M. Ebrahimzadeh, A. De Rossi, M. Calligaro, V. Ortiz, and V. Berger, Appl. Phys. Lett. **83**, 620 (2003).
[12]X. Yu, L. Scaccabarozzi, J. S. Harris, P. S. Kuo, and M. M. Fejer, Opt. Express **13**, 10742 (2005).
[13]A. De Rossi and V. Berger, Phys. Rev. Lett. **88**, 043901 (2002).
[14]P. Abolghasem, J. B. Han, D. Kang, B. J. Bijlani, and A. S. Helmy, IEEE J. Sel. Top. Quantum Electron. **18**, 812 (2012).
[15]R. Horn, P. Abolghasem, B. J. Bijlani, D. Kang, A. S. Helmy, and G. Weihs, Phys. Rev. Lett. **108**, 153605 (2012).
[16]B. J. Bijlani and A. S. Helmy, Opt. Lett. **34**, 3734 (2009).
[17]C. Tong, B. J. Bijlani, S. Alali, and A. S. Helmy, IEEE J. Quantum Electron. **46**, 1605 (2010).
[18]P. Baldi, M. Sundheimer, K. ElHadi, M. P. deMicheli, and D. B. Ostrowsky, IEEE J. Sel. Top. Quantum Electron. **2**, 385 (1996).
[19]B. R. Bennett, R. A. Soref, and J. A. Delalamo, IEEE J. Quantum Electron. **26**, 113 (1990).
[20]H. A. Zarem, J. A. Lebens, K. B. Nordstrom, P. C. Sercel, S. Sanders, L. E. Eng, A. Yariv, and K. J. Vahala, Appl. Phys. Lett. **55**, 2622 (1989).
[21]S. Gehrsitz, F. K. Reinhart, C. Gourgon, N. Herres, A. Vonlanthen, and H. Sigg, J. Appl. Phys. **87**, 7825 (2000).
[22]W. Susaki, S. Ukawa, and M. Tanaka, Phys. Status Solidi C **3**, 683 (2006).
[23]A. P. Ongstad, D. J. Gallant, and G. C. Dente, Appl. Phys. Lett. **66**, 2730 (1995).
[24]M. Ravaro, M. Le Du, J. P. Likforman, S. Ducci, V. Berger, G. Leo, and X. Marcadet, Appl. Phys. Lett. **91**, 191110 (2007).
[25]L. Chanvillard, P. Aschieri, P. Baldi, D. B. Ostrowsky, M. de Micheli, L. Huang, and D. J. Bamford, Appl. Phys. Lett. **76**, 1089 (2000).
[26]T. Matsushita, I. Ohta, and T. Kondo, Appl. Phys. Express **2**, 061101 (2009).

Downloaded 27 Aug 2013 to 142.150.242.148. This article is copyrighted as indicated in the abstract. Reuse of AIP content is subject to the terms at: http://apl.aip.org/about/rights_and_permissions